

Investigation of a parametric instability between ELF and VLF modes driven by antennas immersed in a cold, magnetized plasma

D. Main*

T2Sys Inc., Beavercreek, Ohio 45431, USA

V. Sotnikov and J. Caplinger

Air Force Research Laboratory (AFRL/RV),

Wright Patterson AFB, Ohio, 45433, USA

D. V. Rose

Voss Scientific, Albuquerque, New Mexico 87108

(Dated: April 6, 2024)

Abstract

We have studied the behavior of a VLF, ELF and combined ELF/VLF antenna immersed in a cold, magnetized plasma using a fully kinetic, three dimensional Particle-in-Cell simulation code called Large Scale Plasma (LSP). All the antennas are modeled as magnetic dipoles ($\rho_{ant} = 0$) and are assigned a time varying current density within a finite sized current loop. The VLF antenna is driven at 10 Amps with a frequency (ω_{VLF}) greater than the lower hybrid frequency (ω_{LH}), while the ELF antenna is driven at 3 Amps with a frequency (ω_{ELF}) less than ω_{LH} . The combined ELF/VLF antenna (which we call a parametric antenna) includes both antennas driven simultaneously in the same simulation domain. We show that the parametric antenna non-linearly excites electromagnetic (EM) Whistler waves to a greater extent than the VLF antenna alone. We also show that the parametric excitation of EM Whistler waves leads to greater emitted EM power (measured in Watts) compared with a VLF antenna alone.

Whistler waves are ubiquitous in the space environment and have been observed in the magnetotail [1], ionosphere [2], solar wind [3], other planets [4, 5] and numerous laboratory experiments [6]. Some of the earliest observations of whistler waves were correlated with lightning strikes in which the whistler wave is guided by an ionospheric duct [7]. An important aspect of whistler waves is that they are known to cause pitch angle scattering of highly energetic electrons, for example, in Earth's radiation belt [8]. Furthermore, EM whistler waves weakly decay from their source region and travel great distances along the background magnetic field. The group velocity (and hence the energy) of the EM whistler travels in a cone with a peak angle of 19.5° w.r.t. Earth's magnetic field, which is known as the shadow boundary and is determined by the long wavelength inflection point in the dispersion relation [9]. Therefore, as whistler waves propagate great distances along Earth's magnetic field, they carry with it energy that pitch angle scatter highly energetic particles, causing these particles to violate the frozen in condition.

One method for generating whistler waves in a cold, magnetized plasma is with a magnetic or electric loop antenna driven in the frequency range $\omega_{LH} < \omega_{VLF} \ll \omega_{ce}$ [10, 11], which we call a VLF antenna and ω_{ce} is the electron cyclotron frequency. In a magnetic loop antenna [12] the charge density in the antenna (ρ_{ant}) equals 0 and the current density varies with time at frequency ω . In an electric loop antenna $\rho_{ant} \neq 0$ and the charge density varies spatially with frequency ω . It has been shown [12] that the two are equivalent and both result in singularities in the electric field within a cone of angle θ_c measured off the magnetic field direction, though the electric field singularity is stronger in the electric loop antenna. In a plasma with no dissipation, the resonance cones form at an angle given by

$$\sin^2(\theta_c) = \frac{\omega_{VLF}^2 (\omega_{pe}^2 + \omega_{ce}^2 - \omega_{VLF}^2)}{\omega_{pe}^2 \omega_{ce}^2} \quad (1)$$

In a plasma with dissipation, the singularities become finite within the angle θ_c in a spatially localized resonance cone. As noted in previous work, much of the source power due to a VLF antenna is radiated as electrostatic Lower Oblique Resonance (LOR) modes [also referred to as quasi-electrostatic whistler waves] which decay as R^{-1} (R is the distance from the antenna) away from the source antenna, whereas the EM whistler wave decays as $R^{-1/2}$ [9]. Considerable experimental work has shown that the loop antennas driven within

the frequency range $\omega_{LH} < \omega \ll \omega_{ce}$ form LOR waves as expected [13]. However, in these efforts, it is not clear how much of the power is radiated as EM whistler waves compared with the LOR modes.

One method that has been proposed to increase the wave power in the EM whistler wave is through a parametric interaction between LOR modes and a low frequency density perturbation generated by a dipole antenna which excites ion sound waves [9, 14]. In this paper, we generate a low frequency density perturbation with a loop antenna and excite ELF waves instead ion sound waves. We call the low frequency loop antenna an ELF antenna which is driven at a frequency $\omega_{ELF} < \omega_{LH}$, and show below that the ELF antenna drives a fast magnetosonic wave which causes the low frequency density perturbation. We call an antenna consisting of a combined ELF and VLF antenna (occupying the same volume but driven at two different frequencies) a parametric antenna. We demonstrate in this paper an increase in the EM whistler wave power in the parametric antenna simulation compared with the simulation of a VLF antenna alone and attribute this increase in wave power to a parametric interaction between the LOR modes and a low frequency density perturbation. We find in the parametric antenna that whistler waves are excited on combination frequencies $\omega_{VLF} \pm \omega_{ELF}$, as expected from theoretical work.

We now describe the 3D simulation set up for three different antennas immersed in a magnetized plasma. We have performed three different fully kinetic simulations which we call Run 1, Run 2, and Run 3. Run 1 contains the ELF antenna, Run 2 contains the VLF antenna, and Run 3 contains the parametric antenna. All three antennas are identical except the frequency at which they are driven. Besides the different antennas, all three runs are identical. We present results that demonstrate the formation of resonance cones at angles consistent with theory and the non-linear excitation of EM whistler waves in the parametric antenna simulation. Furthermore, we will compare wave spectra with linear theory to demonstrate that the wave structures that form in the three separate simulations are consistent with theory. The simulation domain is established in a Cartesian volume such that $-600 \text{ m} < x, y < 600 \text{ m}$ and $-750 \text{ m} < z < 750 \text{ m}$, where x and y are perpendicular to the external magnetic field and z is parallel. The number of cells used is $n_x = n_y = 600$ and $n_z = 750$ so that the grid size in all dimensions is 2 m. The spatial grid size was chosen based on trial 2D simulations in which we varied the grid size and compared the evolved

field structures. In these different runs, we set the grid size to 0.50 m, 1 m, 2 m and 4 m. We find good agreement with linear theory in the different 2D runs up to a grid size of 2 m. Therefore, for the 3D runs, we chose to use the 2 m grid size due to computational constraints. For these simulation, we use 8 plasma particles per cell (4 electrons, 4 ions), for a total of $\sim 2.2 \times 10^9$ particles. The mass ratio of ions to electrons is 1836:1, so that these simulations are assuming the ion species is hydrogen. We use an implicit, energy conserving algorithm to provide the Lorentz force particle push and also to solve for the self-consistent EM fields [15, 16]. The time step (dt) used is 3 times the CFL limited time step, which equates to a value of $dt \approx 11$ ns. This time step was chosen by varying it from 1 to 5 times the CFL limited time step in otherwise equivalent 2D simulations. Above 3 times the CFL limited timestep, noticeable difference were observed in the evolved field structures.

The plasma parameters for the simulation results presented in this paper are the following: The background electron and ion density is 10^5 cm^{-3} . The background magnetic field points in the z-direction and is 0.30 Gauss. We assume hydrogen ions. The temperature of the plasma is set to 0 which reduces the numerical noise in the simulation. We have performed simulations with a finite temperature and achieve similar results to the ones presented here. Furthermore, by setting the plasma temperature to 0, we do not need to replace particles that can leave the simulation through the outlet boundaries (discussed in the next paragraph). We have set $\omega_{VLF} = 1.31 \times 10^6 \text{ rad/s} \approx 11\omega_{LH}$ and $\omega_{ELF} = 1.04 \times 10^5 \text{ rad/s} \approx 0.88\omega_{LH}$.

The simulation uses outlet boundaries [17] which attempt to match the outgoing plasma waves in the simulation domain with a virtual wave that forms outside the simulation domain. This matching condition allows the wave to propagate out of the simulation domain and minimizes reflections back into the simulation domain. We construct a loop antenna in the center of the simulation domain using a volume model in LSP. This volume model generates a uniform dipole current with a set frequency within a fixed volume of space and therefore, via Maxwell's equation, generates a dipole electric field. However, the volume model only allows us to define a dipole electric field in a solid region. To construct a dipole loop, we glue four solid volumes together with each volume composing a side of a cube loop (this is analogous to a square donut). At the four corners, we superimpose

conducting volumes which we find reproduces better the Lower Oblique Resonance cones. The antenna is placed in the center of the simulation domain such that the normal vector to the loop antenna lies in the z -direction (which is also the direction of the external magnetic field). Therefore, the plane of the loop lies in the $x - y$ plane. The square antenna has an inner width (which represents the hollow portion) of 700 cm and an outer width of 1100 cm so that the thickness of the antenna is 400 cm. In the z -direction, the thickness is 1100 cm.

In Figure 1 we show a 2D slice of the LOR cones. The angle that these structures form is consistent with theory [10] and is found to be $\sim 15^\circ$ for the plasma parameters that we have used. We varied ω_{VLF} in 2D simulations (in the x - z plane) and we find the resonance cones form at a smaller angle when ω_{VLF} decreases, consistent with Equation 1. Therefore, it is clear that we can reproduce the resonance cones discussed in previous experimental and theoretical results. However, because these waves have a large electrostatic component, the $\vec{J} \cdot \vec{E}$ power generated does not propagate far from the antenna. The goal of this paper is to demonstrate, using a fully kinetic PIC model that we can parametrically couple the electrostatic LOR waves with the electromagnetic magnetosonic waves and pump additional power into the electromagnetic whistler waves.

Prior research [9, 14] has discussed in greater depth the dispersion curve for the EM whistler and ES Lower Oblique modes. As discussed in these papers for values of $k_\perp \ll \omega_{pe}/c$ (c is the speed of light and k_\perp is the wave vector perpendicular to the external magnetic field), the wave is electromagnetic and for $k_\perp \gg \frac{\omega_{pe}}{c}$ the wave is electrostatic. Therefore, the LOR waves have values of $k_\perp \gg \omega_{pe}/c$. The strict upper limit on the value of k_\perp above which the wave is quasi-electrostatic is known as the shadow boundary which is the long wavelength inflection point of the refractive index surface. However, this corresponds to a value of $k_\perp \approx 0.1\omega_{pe}/c$, and therefore the purely EM whistler mode resides in the range $0 < k_\perp \lesssim 0.1\omega_{pe}/c$, which requires exceedingly large computational domains to resolve. Furthermore, according to Equations (4) and (5) from *Fiala et. al.* [9], the ES portion of the dispersion curve is linear in k_z . We find that the linear portion of the dispersion curve starts near $k_\perp = \omega_{pe}/c$. Therefore, in this paper, we define waves with $k_\perp < \omega_{pe}/c$ to be EM and $k_\perp > \omega_{pe}/c$ to be ES, which is obviously an approximation, but a necessary one due to our limited computing resources. To calculate the EM wave power

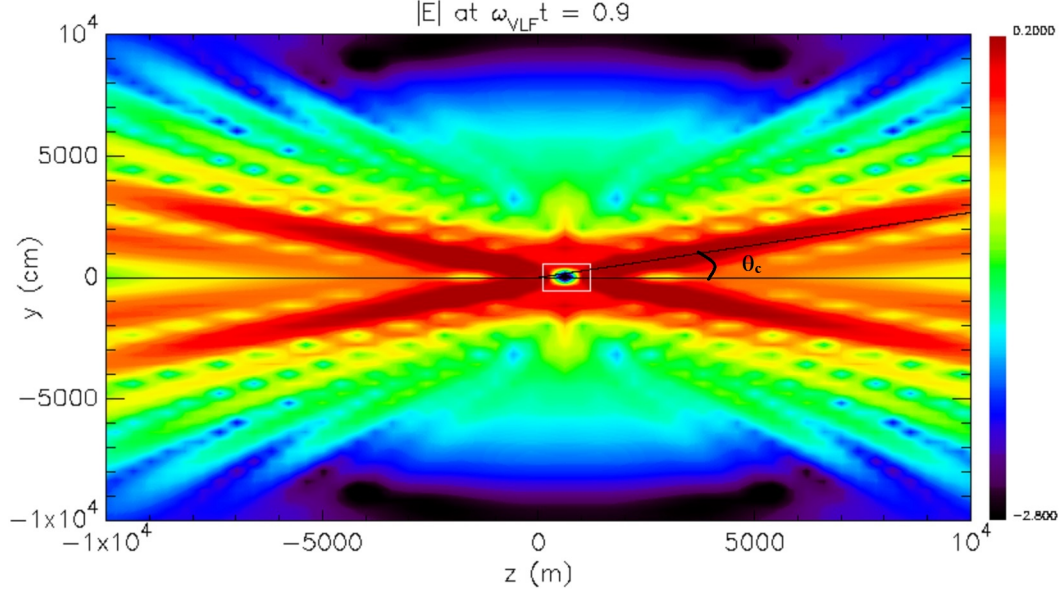


FIG. 1: Magnitude of the electric field early in the parametric antenna simulation showing the formation of the LOR cones. The black square represents the antenna. Note that only a portion of the simulation domain is shown in this Figure. The magnetic field is in the z-direction.

(measured in Watts), we have developed a k-space filter which allows us to calculate the EM contribution to the electric fields (\vec{E}) and current density (\vec{J}). Essentially, we calculate the Fourier Transform (FT) of the fields such that $\text{FT}\{\vec{E}(x, y, z)\} = \vec{\mathcal{E}}(k_x, k_y, k_z)$ and $\text{FT}\{\vec{J}(x, y, z)\} = \vec{\mathcal{J}}(k_x, k_y, k_z)$. Next we set $k_\perp^2 = k_x^2 + k_y^2$ and invoke a filter in k-space according to the following equations:

$$\vec{\mathcal{E}}_{EM}(\vec{k}) = \begin{cases} \vec{\mathcal{E}}(\vec{k}) & \text{if } k_\perp < \frac{\omega_{ce}}{c} \\ 0 & \text{if } k_\perp > \frac{\omega_{ce}}{c} \end{cases} \quad (2)$$

$$\vec{\mathcal{E}}_{ES}(\vec{k}) = \begin{cases} \vec{\mathcal{E}}(\vec{k}) & \text{if } k_\perp > \frac{\omega_{ce}}{c} \\ 0 & \text{if } k_\perp < \frac{\omega_{ce}}{c} \end{cases} \quad (3)$$

Where the subscript EM/ES denotes electromagnetic and electrostatic portion of the field. The same filter is applied to the self-consistent current density, $\vec{\mathcal{J}}$. Note that in Equations 2 and 3, all values of k_\parallel are included in the EM and ES portions of the E- and J-fields. We next compute the power due to the EM portion of the fields, which we demonstrate below

is mainly due to the EM Whistler wave based on the good agreement between the Whistler dispersion and the Fourier spectrum of the electric field. We use the following equation to compute the power:

$$P_{EM} = \frac{1}{2} \int \vec{\mathcal{E}}_{EM} \cdot \vec{\mathcal{J}}_{EM}^* + \vec{\mathcal{E}}_{EM}^* \cdot \vec{\mathcal{J}}_{EM} d^3k \quad (4)$$

Where the * indicates complex conjugate. In order to compare Equation 4 with the theoretical output of the antenna, we have also computed the $\vec{J} \cdot \vec{E}$ power from the antenna in the following way:

$$P_{Ant} = \frac{1}{2} \int \vec{\mathcal{E}}_{EM} \cdot \vec{\mathcal{J}}_{Ant}^* + \vec{\mathcal{E}}_{EM}^* \cdot \vec{\mathcal{J}}_{Ant} d^3k \quad (5)$$

where $\vec{\mathcal{J}}_{Ant}$ is the FT of the current density in the antenna. Of course, Equations 4 and 5 are nearly identical. Essentially, in using Equation 4, we are only considering the power which is non-linearly pumped into the EM fields by the plasma currents which act as a large antenna driven by the parametric instability. The lower bound on the integrals in Equations 4 and 5 is limited by the perpendicular box size, which is 1200 m in our simulation. Therefore, the lower bound is $\sim 0.08\omega_{pe}/c$ and the upper bound is ω_{pe}/c due to Equation 2

We have performed two simulations with only ELF antennas, one driven at 1 Amp and the other driven at 3 Amps. We have also performed a simulation with only a VLF antenna driven at 10 Amps. Finally, we performed two simulations with a parametric antenna such that the ELF/VLF currents are 1 Amp/10 Amps and 3 Amps/10 Amps. We find little difference between the 1 Amp/10 Amp parametric antenna simulation and the 10 Amp VLF antenna simulation, indicating that there is little non-linear interaction between the LOR modes and density perturbations driven by the ELF antenna in this case. Therefore, all results discussed in the remainder of this paper are for the 3 Amp/10 Amp parametric antenna simulation. We expect the ELF antenna to drive Fast Magnetosonic (FM) waves which has a dispersion equation given by Equation (3) in *Sagdeev et. al.* [18]. We show in Figure 2 the k -space spectra from the ELF simulation with the white curve representing the solution to the FM dispersion in *Sagdeev et. al.* [18]. The good fit between the linear dispersion curve and the power spectra from the simulation indicates that we are resolving the necessary wave numbers to drive the FM mode.

For comparison, the results of the two calculations from Equations 4 and 5 are shown in Figure 3. We saved the full 3D electric field, magnetic field, and current density every 200

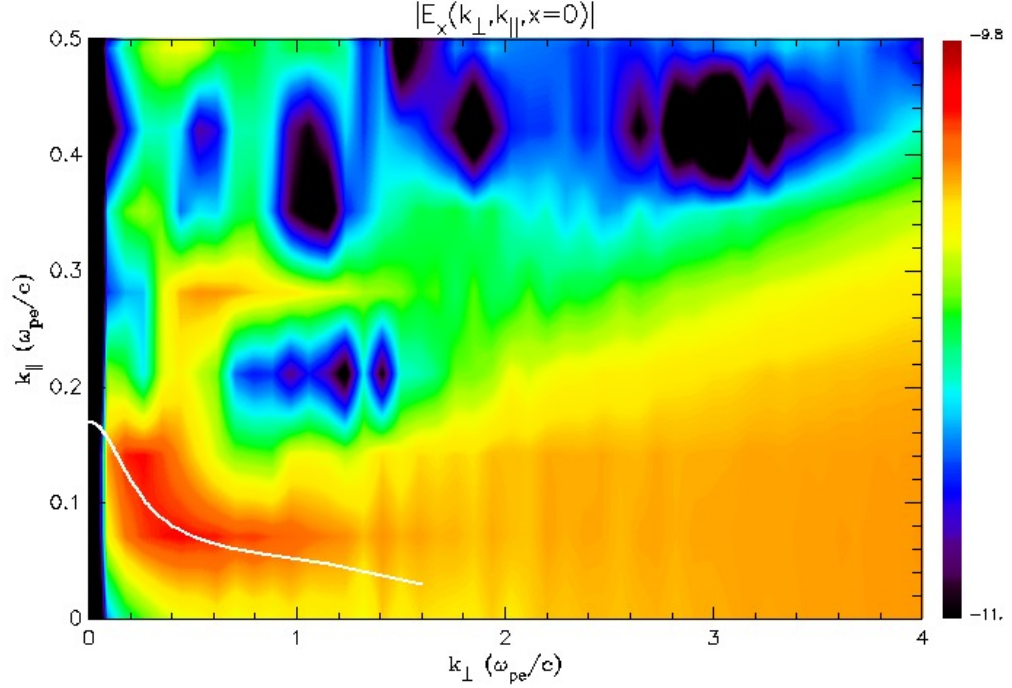


FIG. 2: The wave power calculated from E_x through the $x=0$ plane from the 3 Amp ELF simulation at ~ 0.20 ELF periods. The white curve represents the solution to the FM dispersion relation.

time steps, which allows us to resolve 2 data points per VLF period and 26 data points per ELF period. We ran the parametric simulation for about 80000 time steps, which is about 15 ELF periods. The simulations were performed on massively parallel computing clusters using several thousand processors and took about 15 days. To compare the parametric run with the 10 Amp/3 Amp antenna, we also ran a VLF simulation (driven at 10 Amps) and an ELF simulation (driven at 3 Amps) with identical simulation domain sizes, grid sizes and time steps. This has allowed us to compare the linear and non-linear evolution of the plasma. Because the calculation from the VLF and ELF simulations show that the power output from the antenna level off more quickly than the parametric antenna simulation, we ran these two simulation for 50000 time steps. We note an oscillatory trend to all three data sets, with a frequency of $\sim \omega_{ELF}$. However, given that the VLF simulation is independent of the ELF frequency, we surmise that we are driving a fundamental FM mode in the plasma nearly independent of the ELF driving frequency. We tested this idea by performing another parametric simulation in which the ELF antenna is driven at \sim

$0.52\omega_{LH}$) (i.e. $\sim 60\%$ of the original frequency) and indeed find the same periodicity in the power calculation, demonstrating that the fundamental frequency is independent of the driving frequency. We have averaged over 1 ELF period to smooth the oscillation and demonstrate an increase in average power in the parametric antenna. This is shown as the dashed curves in Figure 3. The red curves in Figure 3 represents the superposition of the linear power generated by the ELF and VLF antennas run independently. In comparing the power generated by the superposition of the ELF and VLF antennas and the parametric antenna, we note a factor of 3 increase in power. Not all the power generated by the antenna radiates away from the antenna. Some of the power generates ES waves and some of it heats the plasma, neither of which are accounted for in Equations 4 and 5. We have calculated the EM wave power from the VLF simulation alone using Equation 4 and also show this calculation as the blue curve in Figure 3 and note a factor of 7 gain between the VLF and parametric antennas.

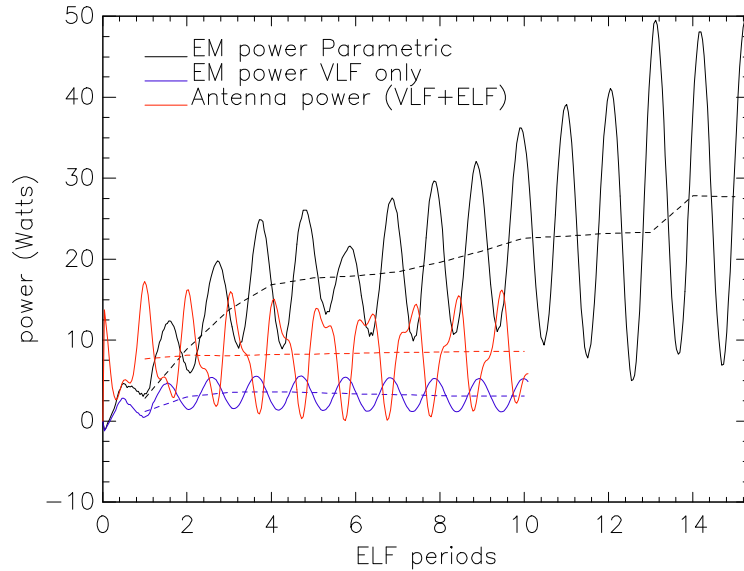


FIG. 3: EM power calculation (blue and black curves) using Equation 4 and the power generated by the antenna (red) using Equation 5. The dashed curve represents the average over one ELF period.

To demonstrate that the increase in power observed in Figure 3 is in fact due to EM whistler waves, we show wave spectra (FT of field components) in the $y - z$ plane from the 10 Amp VLF simulation, and the 10 Amp/3 Amp parametric simulation. Based on previously developed theories [9, 14], we infer that the best explanation for the observed increase in the EM whistler wave power is due to a parametric interaction between the

FM wave and the LOR resonance waves. The whistler dispersion from *Fiala et. al.* [9] is compared with wave power from the VLF and parametric simulations in all four panels. Panels (a) and (b) represent the FT of E_x in the y-z plane at $x = 40$ m and Panels (c) and (d) represent the FT of E_z in the y-z plane at $x = 400$ m. The two left panels are from the VLF simulation and the two right panels are from the parametric simulation. According to [9], for $k_{\perp} \ll \omega_{pe}/c$, the wave corresponds to the EM whistler wave and for $k_{\perp} \gg \omega_{pe}/c$, the wave corresponds to the LOR. Therefore, if we are exciting the EM whistler in the parametric antenna simulation, then we expect to observe smaller wave numbers excited. In comparing the VLF (left two panels) and parametric simulations (right two panels) we observe that both follow the whistler dispersion curve well. However, in the parametric simulation, we also see that lower wave number modes have a greater wave power compared with the VLF antenna alone. Close to the antenna at $x=40$ m [the antenna is placed close to the center of the simulation domain which is at the coordinates (0,0,0)], we see large EM wave power in both the VLF and parametric antenna. Though difficult to see from the color scale, the average wave power in the parametric antenna is ~ 2 times greater than the VLF antenna. However, it is very obvious that far from the antenna at $x=400$ m, the waves are dominated by the EM whistler wave and that the parametric antenna wave power is much larger than the VLF wave power (~ 10 times greater).

Finally, we compare the non-linear wave amplitudes excited in the parametric simulation with the linear wave amplitudes. We define the linear fields as the superposition of the fields from the separate ELF and VLF simulation, and the non-linear fields as the total field from the parametric simulation minus the fields from the separate ELF and VLF simulations: equation:

$$\begin{aligned} E_L &= E_{VLF} + E_{ELF} \\ E_{NL} &= E_{par} - E_L \end{aligned} \tag{6}$$

Where E denotes the electric field. The same definition can be written for all the field quantities. We show E_x and B_y for both the linear and non-linear fields in Figure 5. Note that only a portion of the simulation domain is plotted. Notice in both runs considerable wave activity along the external magnetic field on the same axis as the antenna at the center of the figures. However, in the NL fields, we notice off-axis waves that fill the simulation domain that are not present in the linear fields. We attribute these off-axis

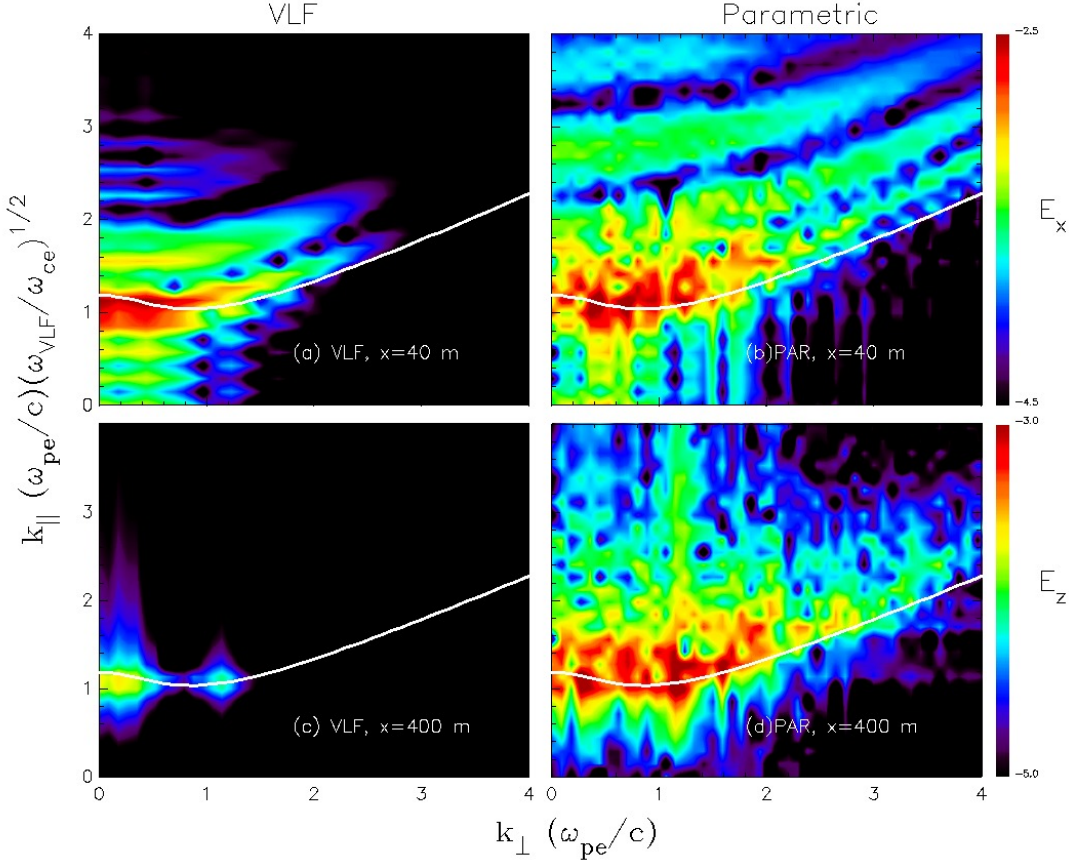


FIG. 4: (a,b) Wave power from the VLF (panel a) and parametric (panel b) simulations computed from E_x at $x=40$ m. (c,d) wave power from E_z at $x=400$ m from the VLF (panel c) and parametric (panel d) simulation. All data are from time step 46200 (~ 9 ELF periods).

waves to the EM whistler waves excited by the parametric interaction between the LOR waves and the FM waves. This interpretation is consistent with Figure 4 which shows that far from the antenna there is considerable EM whistler wave power in the parametric antenna compared with VLF antenna. Figure 5a demonstrates that significant non-linear wave activity occurs in the parametric antenna simulation and Figure 5aa shows that these waves have a strong magnetic field component, consistent with interpretation that these off-axis waves are EM.

In conclusion, we have shown that a parametric interaction between electrostatic LOR modes excited by a VLF antenna and FM modes excited by an ELF antenna leads to the non-linear excitation of electromagnetic whistler waves. While a VLF antenna alone also excites EM whistler waves, the parametric antenna non-linearly pumps more power

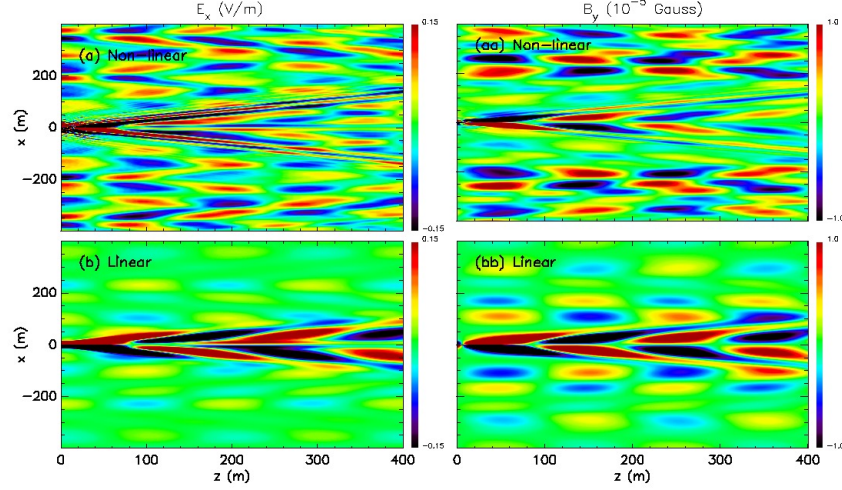


FIG. 5: (a,aa) Non-linear electric and magnetic field from the parametric antenna simulation as defined in Equation 6. (b,bb) Linear electric and magnetic fields also defined in Equation 6. All panels are plotted at time step 46200 (~ 9 ELF periods).

(measured in Watts) into the EM whistler mode compared with a VLF antenna alone. We find evidence for the existence of EM whistler modes in k -space and real space. Furthermore, we have also investigated the non-linear excitation of wave modes in frequency space at $\omega_{VLF} \pm \omega_{ELF}$ at different spatial locations in the simulation domain. We indeed find evidence that the combination frequency is excited, as expected from theory [9]. This antenna could be used, for example, to generate EM whistler waves from a remote antenna to pitch angle scatter high energy particles away from satellites which may be subjected to such a harsh environment.

* daniel.main@gmail.com

- [1] H. Viberg, Y. V. Khotyaintsev, A. Vaivads, M. André, H. S. Fu, and N. Cornilleau-Wehrlin, *Journal of Geophysical Research (Space Physics)* **119**, 2605 (2014).
- [2] M. Spasojevic, *Journal of Geophysical Research (Space Physics)* **121**, 7547 (2016).

- [3] S. P. Gary, E. E. Scime, J. L. Phillips, and W. C. Feldman, J. Geophys. Res. **99**, 23 (1994).
- [4] Y. Hobara, O. A. Molchanov, M. Hayakawa, and K. Ohta, J. Geophys. Res. **100**, 23523 (1995).
- [5] D. S. Orłowski and C. T. Russell, Advances in Space Research **16** (1995), 10.1016/0273-1177(95)00220-9.
- [6] R. L. Stenzel, jgr **104**, 14379 (1999).
- [7] R. L. Smith, J. Geophys. Res. **66**, 3699 (1961).
- [8] D. Mourenas, A. V. Artemyev, Q. Ma, O. V. Agapitov, and W. Li, Geophys. Res. Lett. **43**, 4155 (2016).
- [9] V. Fiala, E. N. Kruchina, and V. I. Sotnikov, Plasma Physics and Controlled Fusion **29**, 1511 (1987).
- [10] R. K. Fisher and R. W. Gould, Physics of Fluids **14**, 857 (1971).
- [11] T. N. C. Wang and T. F. Bell, J. Geophys. Res. **77**, 1174 (1972).
- [12] V. I. Karpman, Physics Letters A **117**, 73 (1986).
- [13] J. M. Urrutia and R. L. Stenzel, Physics of Plasmas **21**, 122107 (2014).
- [14] V. I. Sotnikov, G. I. Solov'yev, M. Ashour-Abdalla, D. Schriver, and V. Fiala, Radio Science **28**, 1087 (1993).
- [15] D. R. Welch, D. V. Rose, R. E. Clark, T. C. Genoni, and T. P. Hughes, Computer Physics Communications **164**, 183 (2004).
- [16] D. R. Welch, D. V. Rose, M. E. Cuneo, R. B. Campbell, and T. A. Mehlhorn, Physics of Plasmas **13**, 063105 (2006).
- [17] C. K. Birdsall and A. B. Langdon, *Plasma Physics Via Computer Simulation*, Series in Plasma Physics (Taylor and Francis, 2005).
- [18] R. Z. Sagdeev, V. I. Sotnikov, V. D. Shapiro, and V. I. Shevchenko, ZhETF Pisma Redaktsiiu **26**, 747 (1977).